

Article

# Experimental Deployment of Microbial Mineral Carbonation at an Asbestos Mine: Potential Applications to Carbon Storage and Tailings Stabilization

Jenine McCutcheon <sup>1,2,\*</sup> , Connor C. Turvey <sup>3</sup> , Sasha Wilson <sup>3</sup>, Jessica L. Hamilton <sup>3</sup>  and Gordon Southam <sup>1</sup>

<sup>1</sup> School of Earth & Environmental Sciences, The University of Queensland, St. Lucia, QLD 4072, Australia; g.southam@uq.edu.au

<sup>2</sup> School of Earth and Environment, The University of Leeds, Leeds LS2 9JT, UK

<sup>3</sup> School of Earth, Atmosphere and Environment, Monash University, Clayton, Melbourne, VIC 3800, Australia; connor.turvey@monash.edu (C.C.T.); sasha.wilson@monash.edu (S.W.); jessica.hamilton@monash.edu (J.L.H.)

\* Correspondence: j.mccutcheon@leeds.ac.uk; Tel.: +44-113-343-2846

Received: 30 August 2017; Accepted: 6 October 2017; Published: 12 October 2017

**Abstract:** A microbial mineral carbonation trial was conducted at the Woodsreef Asbestos Mine (NSW, Australia) to test cyanobacteria-accelerated Mg-carbonate mineral precipitation in mine tailings. The experiment aimed to produce a carbonate crust on the tailings pile surface using atmospheric carbon dioxide and magnesium from serpentine minerals (asbestiform chrysotile;  $Mg_3Si_2O_5(OH)_4$ ) and brucite [ $Mg(OH)_2$ ]. The crust would serve two purposes: Sequestering carbon and stabilizing the hazardous tailings. Two plots ( $0.5\text{ m}^3$ ) on the tailings pile were treated with sulfuric acid prior to one plot being inoculated with a cyanobacteria-dominated consortium enriched from the mine pit lakes. After 11 weeks, mineral abundances in control and treated tailings were quantified by Rietveld refinement of powder X-ray diffraction data. Both treated plots possessed pyroaurite [ $Mg_6Fe_2(CO_3)(OH)_{16}\cdot 4H_2O$ ] at 2 cm depth, made visible by its orange-red color. The inoculated plot exhibited an increase in the hydromagnesite [ $Mg_5(CO_3)_4(OH)_2\cdot 4H_2O$ ] content from 2–4 cm depth. The degree of mineral carbonation was limited compared to previous experiments, revealing the difficulty of transitioning from laboratory conditions to mine-site mineral carbonation. Water and carbon availability were limiting factors for mineral carbonation. Overcoming these limitations and enhancing microbial activity could make microbial carbonation a viable strategy for carbon sequestration in mine tailings.

**Keywords:** mineral carbonation; mine tailings; chrysotile asbestos;  $CO_2$  storage; cement precipitation; carbonate minerals; microbial carbonation; cyanobacteria

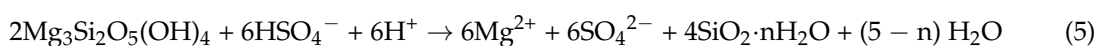
## 1. Introduction

Mineral carbonation has been presented as a strategy for offsetting anthropogenic carbon dioxide ( $CO_2$ ) emissions [1–3], in part because it provides a safe, long-term carbon reservoir for large quantities of  $CO_2$  [1]. Numerous mineral carbonation mechanisms have been investigated for use on ultramafic minerals in ophiolites and mine waste products [4–15]. Natural “passive” carbonation of mine tailings has been documented at several mine sites [7,8,15–18], and could be enhanced by increasing exposure of the tailings to atmospheric  $CO_2$  through aeration of the tailings or altering the tailing deposition rate [9,19,20]. Using ultramafic mine tailings produced by chrysotile, diamond, nickel, chromite,

and platinum group element mines [8,21] as feedstocks for carbonation gives value to these waste products and allows mining companies to partially offset their operational carbon emissions.

Asbestos mine tailings are found at numerous active and historic mine sites worldwide [8,15,17,21–23]. Mining activity has ceased at many of these locations; however, megatons of tailings containing asbestiform minerals remain, posing a threat to the health of nearby residents [24] and polluting natural waterways [22]. Although the mineralogy of the tailings at derelict asbestos mines is well characterized [8,21,25], and asbestos mineral hazard-assessment guidelines are available [26,27], the challenge of remediating this industrial waste remains unsolved. Targeting asbestos mine tailings as a feedstock for mineral carbonation has the potential to aid in tailings containment and remediation with the added value of offsetting carbon emissions.

Laboratory-scale investigations have demonstrated carbonate mineral formation from mine tailings using biologically mediated and abiotic mechanisms [14,28–30]. Microorganisms, particularly cyanobacteria [31–36] and ureolytic bacteria [37,38], can enable carbonate mineral precipitation reactions. Cyanobacteria mediate carbonate mineral precipitation by increasing the pH and alkalinity of the extracellular medium through photosynthesis (Reactions 1–4) [39,40]. These organisms also generate extracellular polymeric substances (EPS) capable of providing nucleation sites for carbonate minerals [41,42]. The conditions resulting from this combination of water chemistry and nucleation template availability facilitates carbonate mineral precipitation in cyanobacteria biofilms and microbial mats. Combining these biogeochemical conditions with the high concentrations of cations that can be generated by leaching ultramafic mine tailings (Reaction 5) can result in mineral carbonation (Reaction 6) [28]. Bioreactors hosting microbial communities capable of precipitating carbonate minerals could be utilized at tailing storage facilities to store anthropogenic CO<sub>2</sub> [19,43].



Adapting microbial carbonation strategies developed in the laboratory for application to a mine site presents a major challenge due to the scale on which the carbonation reactions must be conducted [19]. This investigation is the first of its kind to test the feasibility of implementing microbial carbonation at a mine site, the Woodsreef Asbestos Mine in New South Wales, Australia. If successful, mineral carbonation could serve the dual purpose of remediating and containing the fine-grained hazardous tailings, and storing atmospheric CO<sub>2</sub> [28].

## 2. Materials and Methods

### 2.1. Regional Geology of Woodsreef Mine

The Great Serpentine Belt (GSB) is composed of partially serpentinized harzburgite, massive serpentinite, and schistose serpentinite; and it hosts the Woodsreef Mine (Figure 1) [17,44,45]. Approximately 550,000 t of fibrous chrysotile was mined at this site between 1971 and 1983, producing 75 million t of waste rock and 24.2 million t of tailings that occupy 400 hectares [46,47]. The tailings at Woodsreef primarily consist of serpentine-group minerals (lizardite and minor chrysotile) [Mg<sub>3</sub>Si<sub>2</sub>O<sub>5</sub>(OH)<sub>4</sub>], with minor magnetite (Fe<sub>3</sub>O<sub>4</sub>), chromite (FeCr<sub>2</sub>O<sub>4</sub>), enstatite (MgSiO<sub>3</sub>), forsterite (Mg<sub>2</sub>SiO<sub>4</sub>), calcite (CaCO<sub>3</sub>), quartz (SiO<sub>2</sub>) and brucite [Mg(OH)<sub>2</sub>], with hydromagnesite [Mg<sub>5</sub>(CO<sub>3</sub>)<sub>4</sub>(OH)<sub>2</sub>·4H<sub>2</sub>O] and pyroaurite [Mg<sub>6</sub>Fe<sub>2</sub>(CO<sub>3</sub>)(OH)<sub>16</sub>·4H<sub>2</sub>O] forming as alteration products [17,48].

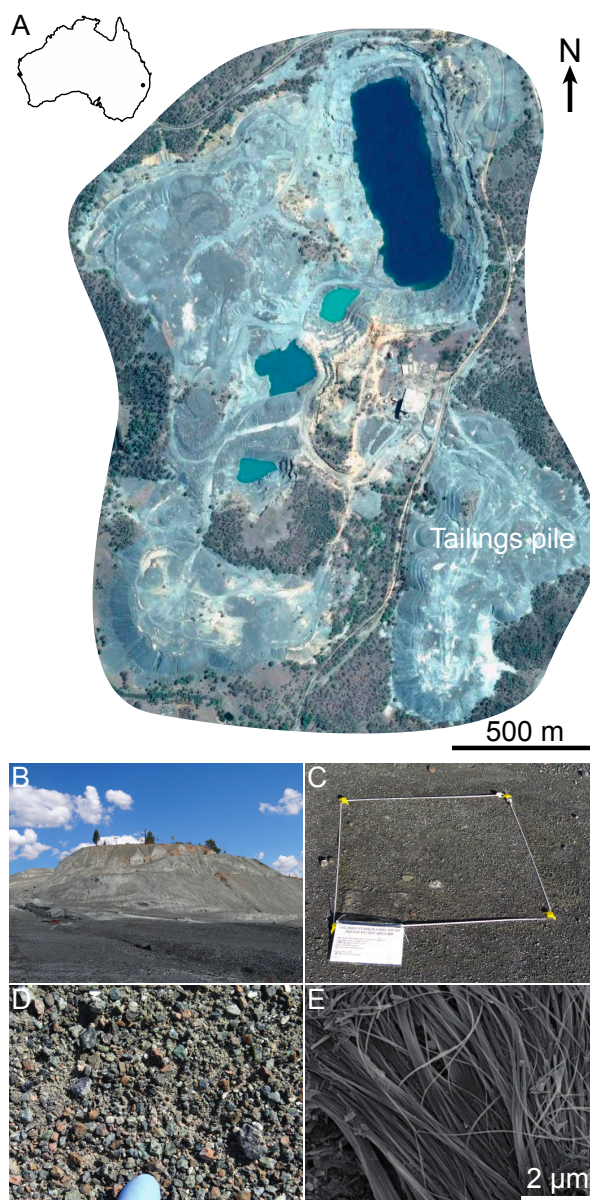


**Figure 1.** (A) Aerial view of Woodsreef Asbestos Mine, New South Wales, Australia (inset) showing the location of the tailings pile. (B) Woodsreef mine hosts 24 million t of asbestos tailings. (C) One of the 1 m × 1 m plots used to study acid dissolution and carbonation of mine tailings. (D) Sub-cm clasts, primarily serpentinite, cover the surface of the tailings pile. (E) Serpentine, including fibrous chrysotile, makes up 90 wt % of the tailings.

## 2.2. Experiment Design

Precipitation of magnesium carbonate minerals was studied in two 1 m × 1 m × 0.5 m (length × width × depth) experimental plots on the Woodsreef Mine tailings pile (Figure 1C). Sulfuric acid was added to both plots with an initial target of leaching magnesium from serpentinite and brucite to a depth of ~1/2 m for 2 weeks; however, the permeability of the tailings limited the volume of solution that could be added to the plots. Local creek water and concentrated H<sub>2</sub>SO<sub>4</sub> were used to make solutions of 0.22 M H<sub>2</sub>SO<sub>4</sub>, of which 40.5 L were added to each plot. The leaching solution likely infiltrated the tailings down to a depth of ~9 cm based on the tailings having an estimated porosity of 29%. This porosity estimate is based on the pore volume calculated in a laboratory study that used the Woodsreef tailings as a starting material to study mineral carbonation in column

experiments [28]. The quantity of acid was selected to maximize magnesium leaching while also maintaining a circumneutral pH [28]. The latter is necessary for the survival of cyanobacteria in the carbonation trial and ultimately carbonate mineral precipitation. The acidified creek water was added slowly to avoid surface runoff onto the tailings surrounding each plot. Note, the sulfuric acid treatment would have also released magnesium and CO<sub>2</sub> from any pre-existing carbonate minerals in the tailings. After 2 weeks, one plot was inoculated with 2 L of a cyanobacteria-dominated consortium (hereafter referred to as the Bio-plot). The consortium was enriched from a biofilm collected from the water in an open pit that remains from mining activity. The inoculum was applied to the plot with 18 L of BG-11 growth medium [49] prepared using local creek water.

The second plot did not receive an inoculum (hereafter referred to as the Chem-plot) and provided a means of characterizing mineral carbonation in acid weathered tailings without the aid of the microbial consortium. A volume of 20 L of creek water was added to the Chem-plot at the 2-week time point to match the solution volume added to the Bio-plot. Both plots were left exposed to the atmosphere under natural conditions for 9 weeks. An adjacent plot of tailings, which were neither leached nor inoculated, was used as a mineralogical baseline for the experiment.

Regional weather data were acquired for the duration of the experiment from a nearby meteorology station (30.38° S, 150.61° E) [50]. Inductively coupled plasma atomic emission spectroscopy (ICP-AES) using a Perkin Elmer Optima 3300 DV (Perkin Elmer, Waltham, MA, USA) and fluid injection analysis (FIA) using a Lachat QuikChem8500 Flow Injection Analyzer (Lachat, Loveland, CO, USA) were used to measure the abundance of cations and nutrients in the creek water, respectively. An HCl titration was used to calculate the alkalinity of the creek water as mg/L HCO<sub>3</sub><sup>-</sup> [51].

### 2.3. Mineralogical Characterization of the Tailings

The mineralogy of the top ~1/2 m of the tailings was characterized using powder X-ray diffraction (XRD) for each stage of the carbonation trial: unreacted tailings, the Chem-plot after 2 weeks, the Chem-plot after 11 weeks, and the Bio-plot after 11 weeks. Each sample set consisted of a depth profile to 47 cm below the surface of the tailings pile as a means of determining how the mineralogy changed with depth and time over the course of the carbonation trial. The depth profiles for the unreacted tailings and the Chem-plot after 2 weeks consisted of triplicate samples (~15 g each) collected from 0–2 cm, 2–17 cm, 17–32 cm, and 32–47 cm; with these depth selections based on macroscopically visible transitions in grain size and mineralogy of the tailings. The 2-week Chem-plot samples were collected from one half of the plot, leaving the other half undisturbed such that it could be sampled at the conclusion of the experiment. After 11 weeks, triplicate samples were collected from both plots at the following depth intervals: 0–2 cm, 2–4 cm, 4–17 cm, 17–32 cm, and 32–47 cm. The tailings from 2–4 cm depth were selected as an additional sampling horizon because they appeared macroscopically different than the adjacent tailings above and below.

Powder X-ray diffraction (XRD) was used to identify the mineral phases in the tailings samples. The samples were air dried for 2 weeks and pulverized. An internal standard of 10 wt % fluorite (CaF<sub>2</sub>) was added to a subsample of each tailings sample. The internal fluorite standard along with structureless pattern fitting (independent of atomic scattering) provided a means of quantifying the abundance of the poorly ordered serpentine in the tailings using the method of Wilson, Raudsepp and Dipple [21].

Each fluorite-doped sample was micronized for 7 min under anhydrous ethanol in a McCrone Micronising Mill using agate grinding elements. The samples were air dried in Petri dishes prior to disaggregation with an agate mortar and pestle. The samples were loaded in back-loading cavity mounts prior to analysis using a Bruker D8 Advance Eco X-ray diffractometer (Bruker, Billerica, MA, USA) with a Cu source operated at 40 kV and 25 mA. Phase identification was completed with reference to the ICDD PDF-2 Release 2015 database using DIFFRAC<sup>plus</sup> Eva v.2 software [52]. Rietveld refinements [53–55] were completed using Topas Version 3 [52] and the fundamental parameters approach [56]. The peaks of both serpentine minerals (lizardite and chrysotile) were fitted using a Pawley phase [57] produced by refinement of a pure specimen of chrysotile and employing the

unit cell and space group for this phase [58]. Once a correct fit was achieved for other major phases, the relative intensities for the serpentine peaks were refined. The refinements did not include a step correcting for preferred orientation because refinements for samples that contain phases with severe preferred orientation are commonly more accurate without such corrections [59].

Samples of the tailings from each experiment time point were characterized using scanning electron microscopy (SEM) in conjunction with elemental analysis using energy dispersive X-ray spectroscopy (EDS). The samples were mounted on stainless steel stubs using adhesive carbon tabs and coated with 10 nm of iridium using a Quorum Q150T S sputter coater prior to being characterized using a JEOL JSM-7100F Field Emission SEM (FE-SEM) (JEOL, Ltd., Akishima, Japan). At the conclusion of the experiment, 1 g of tailings from 0–2 cm and 2–4 cm from both plots were added to BG-11 growth medium [49] as a means of confirming the presence of viable cells.

### 3. Results

#### 3.1. Field Observations

The tailing sampling horizons were based on macroscopic observations made at the beginning of the experiment: 0–2 cm consisted of fine-grained fibrous tailings, 2–17 cm consisted of pebbled-sized grains of serpentinite mixed with fine-grained fibrous tailings, 17–32 cm and 32–47 cm both consisted of fine-grained tailings. These horizons were consistent in the tailing profiles sampled in both plots as well as the control tailings. Acid addition to the tailings caused the rapid formation of an orange-red precipitate similar in appearance to pyroaurite found in the tailings and on the walls of the mine pit. Eleven weeks after leaching, both plots exhibited a ~2 mm-thick, orange horizon of what appeared to be pyroaurite approximately 2 cm below the surface of the tailings (Figure 2).



**Figure 2.** (A) After 11 weeks, a 2 mm-thick horizon of pyroaurite (orange material) formed at a depth of 2 cm in both plots. Below this horizon, a white layer of hydromagnesite was found from 2–4 cm depth (bottom right corner of photograph). (B) Intermixed pyroaurite (orange) and hydromagnesite (white) at the contact between the two horizons in the Bio-plot.

No obvious carbonate crust was observed on the surface of the tailings in either plot at the conclusion of the experiment. The Bio-plot contained a laterally continuous horizon of white material from 2–4 cm depth, and carbonate-coated serpentinite clasts from 4–17 cm. There was no macroscopically visible evidence of microbial growth in the Bio-plot after 11 weeks. The Chem-plot contained a similar, though irregularly distributed, white horizon from 2–4 cm. No such horizon was observed in the unreacted tailings.

A total of 248 mm of rain fell on the site during the experiment, with up to 37 mm falling in a single rain event and periods of no precipitation lasting up to 16 days (Supplementary Materials Figure S1) [50]. The mean daily minimum and maximum temperatures were 15 °C and 31 °C, respectively [50].

The creek water added to the plots had a titration-determined alkalinity of 472.75 mg/L as  $\text{HCO}_3^-$ . Magnesium, sodium and calcium were the most abundant cations, with concentrations of 70.4 ppm, 37.4 ppm, and 29.2 ppm, respectively (Supplementary Materials Table S1). The creek water contained  $\text{PO}_4^{3-}$ ,  $\text{NO}_3^-$ , and  $\text{NO}_2^-$ , at concentrations of 27.4 ppb, 1.2 ppb, and 1.1 ppb, respectively (Supplementary Materials Table S1). Note, since the concentration of magnesium in the creek water is low compared to what can be produced through acid leaching of chrysotile tailings [28], the magnesium added to the plots by way of the creek water is considered to have made a negligible contribution to Mg-mineral carbonation, and is not considered throughout the remainder of the manuscript.

### 3.2. Rietveld Refinement Results

Quantitative XRD data for the unreacted tailings indicate that the surface (0–2 cm) of the tailings pile was composed of 91.2 wt % serpentine (lizardite and minor chrysotile), plus minor amounts of magnetite (3.5 wt %), forsterite (2.3 wt %), pyroaurite (1.3 wt %), enstatite (0.8 wt %), and trace abundances quartz, calcite, and brucite (Table 1). The abundance of serpentine in the Chem- and Bio-plot tailings was slightly lower, containing 90.2 wt % and 90.6 wt % serpentine, respectively. In the depth profile of the unreacted tailings, pyroaurite was most abundant between 2 cm and 17 cm at 2.6 wt % (Table 1). Like pyroaurite, hydromagnesite was most abundant in the tailings sampled from just below the surface, with no hydromagnesite being detected in any of the 0–2 cm tailing samples. Hydromagnesite was present at an abundance of 1.1 wt % in the tailings from 2–17 cm (Table 1). The 2–4 cm horizon contained 1.3 wt %, 1.1 wt %, and 1.9 wt % hydromagnesite in the Chem-plot (2 weeks), Chem-plot (11 weeks), and Bio-plot (11 weeks), respectively.

### 3.3. Electron Microscopy

SEM of the unreacted tailings revealed abundant fibrous chrysotile (Figure 1E). Back-scattered electron SEM of a cross-section of the white horizon found in the Bio-plot from 2–4 cm depth revealed Mg-carbonate cement on serpentinite grains (Figure 3). The cement appears to initially form as meniscus cements at grain contacts, leaving unfilled voids between grains (Figure 3A,B). In some cases, cement has filled the voids generating a laterally continuous crust (Figure 3C,D). Secondary precipitates cementing chrysotile fibers in place were observed using secondary electron (SE-) SEM (Figure 3E,F). Precipitated silica exhibited several morphologies: Sub-micrometer thick coatings on grains that conform to the alignment of the chrysotile fibers (Figure 4A), amorphous botryoidal agglomerates (diameter < 1  $\mu\text{m}$ ) on serpentinite grain surfaces (Figure 4B), and as desiccated crusts of amorphous silica engulfing disarticulated chrysotile fibers (Figure 4C,D). SE-SEM of the sample collected from the pyroaurite horizon at 2 cm depth in the Bio-plot revealed aggregates of anhedral, platy crystals (Figure 5A,B). SE-SEM of the white 2–4 cm horizon in the Bio-plot showed plates of hydromagnesite intermixed with chrysotile fibers (Figure 5C,D). When added to BG-11 growth medium, the tailings from 0–2 cm and 2–4 cm in the Bio-plot exhibited positive growth of filamentous cyanobacteria (Figure 6A,B). No growth occurred in the Chem-plot tailings added to BG-11 growth medium, confirming the absence of viable cyanobacteria.

**Table 1.** Rietveld results for the tailings sampled over the duration of the carbonation trial. Each value is given as an average of triplicate samples. The full dataset and corresponding  $R_{wp}$  values are available in the supplementary information file (Supplementary Materials Tables S2–S5).

Depth Profile	Depth (cm)	Mineral Phase (wt %)									Total
		Serpentine	Pyroaurite	Magnetite	Hydromagnesite	Brucite	Calcite	Forsterite	Enstatite	Quartz	
Unreacted tailings	0–2	91.2	1.3	3.5	0.0	0.1	0.2	2.3	0.8	0.5	100.0
	2–17	88.8	2.6	2.2	1.1	0.3	0.4	2.7	1.5	0.2	100.0
	17–32	90.2	1.9	2.1	0.7	0.2	0.7	2.4	1.7	0.1	100.0
	32–47	90.8	1.3	2.1	0.0	0.4	0.5	2.9	2.0	0.0	100.0
Leached tailings (2 weeks)	0–2	92.7	1.3	2.5	0.2	0.2	0.1	1.7	0.8	0.5	100.0
	2–17	88.6	3.4	2.1	1.3	0.2	0.4	2.3	1.4	0.2	100.0
	17–32	89.1	2.3	2.5	1.2	0.2	0.6	2.8	1.2	0.1	100.0
	32–47	93.2	1.5	1.9	0.3	0.1	0.5	1.7	0.8	0.0	100.0
Leached tailings (11 weeks)	0–2	90.2	1.5	2.8	0.0	0.2	0.2	2.7	1.9	0.5	100.0
	2–4	88.6	2.6	2.2	1.1	0.2	0.3	3.3	1.5	0.3	100.0
	4–17	89.9	2.5	2.4	1.4	0.2	0.4	1.9	1.2	0.1	100.0
	17–32	91.9	1.1	2.2	0.3	0.3	0.5	2.1	1.5	0.0	100.0
	32–47	95.0	0.7	1.9	0.0	0.2	0.5	1.3	0.5	0.0	100.0
Leached and inoculated tailings (11 weeks)	0–2	90.6	0.9	3.2	0.0	0.2	0.2	3.0	1.3	0.6	100.0
	2–4	89.6	2.5	2.1	1.9	0.1	0.4	2.2	0.8	0.4	100.0
	4–17	90.4	2.4	2.0	1.2	0.1	0.7	2.2	1.0	0.0	100.0
	17–32	92.0	1.1	2.1	0.7	0.2	0.5	2.5	0.9	0.0	100.0
	32–47	92.4	1.0	2.3	0.0	0.5	0.6	2.2	1.1	0.0	100.0

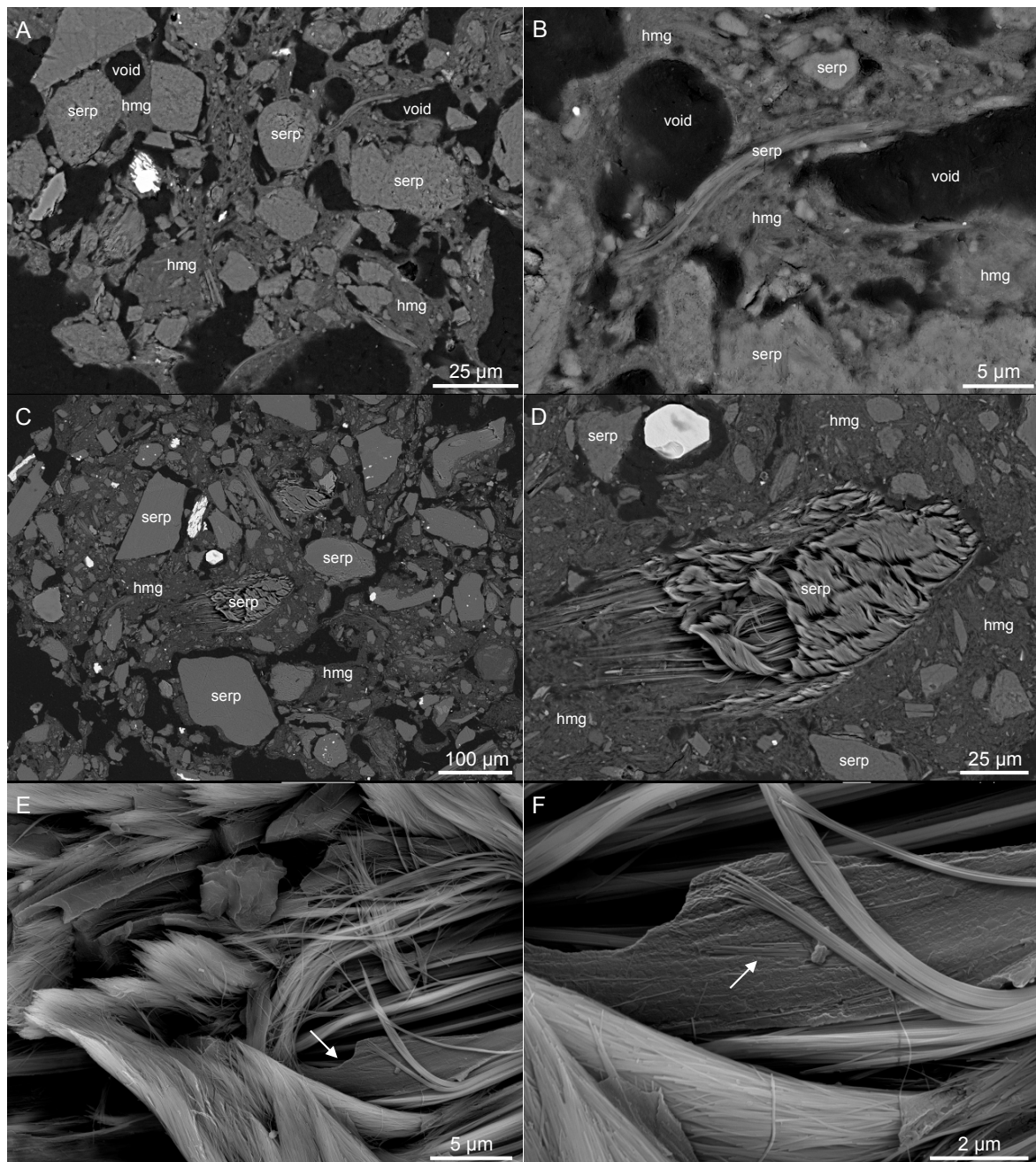


**Figure 3.** Electron micrographs of a cross-section through the carbonate horizon (2–4 cm depth) in the Bio-plot. (A) The hydromagnesite initially formed as meniscus cements at grain contacts. (B) Cements can be observed immobilizing bundles of chrysotile fibers. (C) In some cases, voids are in-filled with hydromagnesite cement. (D) The hydromagnesite cement has immobilized serpentine grains. (E) Cement beginning to form among fibers of chrysotile (arrow). (F) Chrysotile fibers (arrow) enclosed in cement forming within a serpentine grain. Note, hmg: hydromagnesite, serp: serpentine.

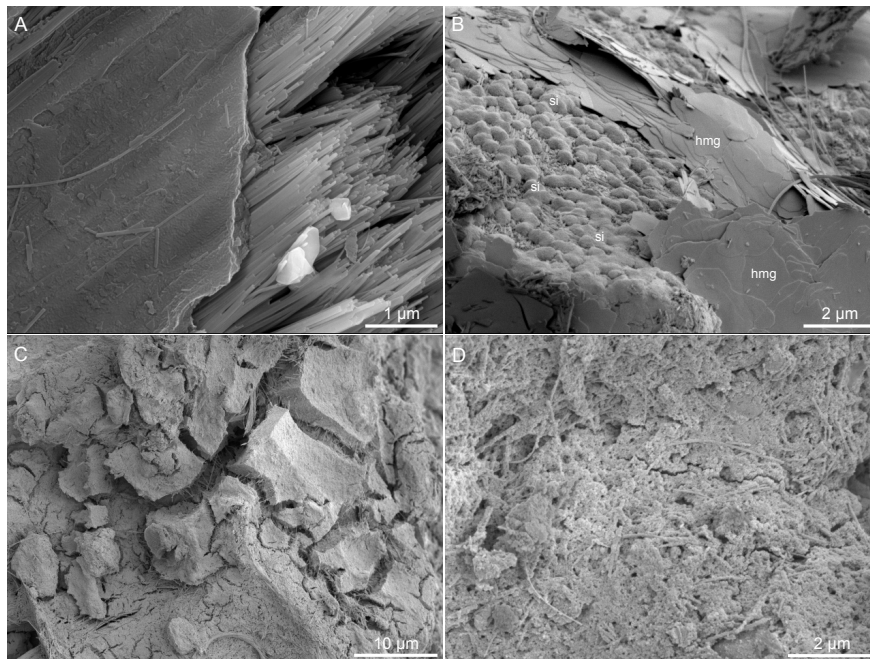


**Figure 4.** Electron micrographs depicting the various morphologies of silica in the Bio-plot. (A) A layer of amorphous silica formed through incongruent dissolution of chrysotile from 2–4 cm depth in the Bio-plot. Note, left side of micrograph: silica, right side of micrograph: chrysotile. (B) Botryoidal silica precipitated on the surface of serpentine grains in the Bio-plot at a depth of 2–4 cm. (C) Desiccated crust of amorphous silica sampled from the 2-cm deep pyroaurite horizon in the Bio-plot, containing chrysotile fibers (D). Note: hmg: hydromagnesite, si: silica.

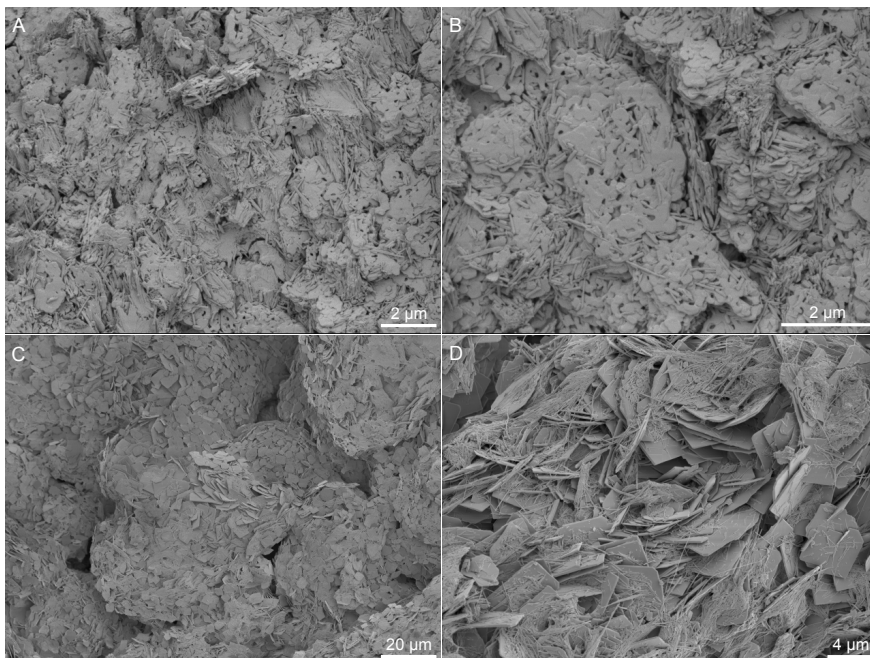


**Figure 5.** SE-SEM micrographs of the pyroaurite horizon found at 2-cm depth in the Bio-plot after 11 weeks showing (A) the relatively poor crystallinity of the pyroaurite indicated by subhedral platelets; and (B) the disarticulated chrysotile fibers found among the pyroaurite crystals. Secondary electron micrographs of the carbonate horizon found from 2–4 cm depth in the Bio-plot after 11 weeks showing (C) the extent of platy hydromagnesite mixed with (D) residual chrysotile fibers.

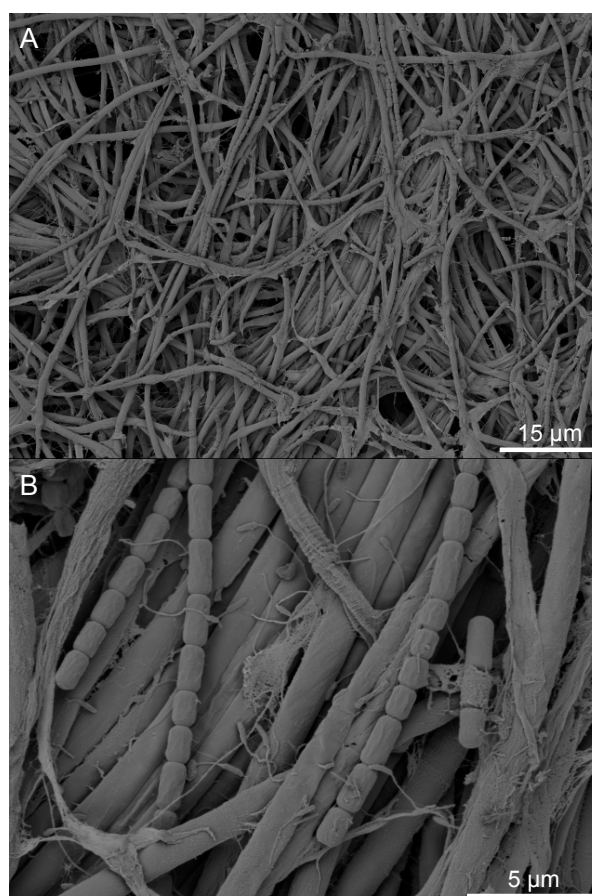


**Figure 6.** (A) SE-SEM micrographs of the biofilm that grew after addition of tailings collected from 0–2 cm depth in the Bio-plot after the 11-week experiment to BG-11 growth medium in the laboratory. (B) The biofilm is composed primarily of filamentous cyanobacteria that can be seen producing small quantities of mesh-like exopolymer.

## 4. Discussion

### 4.1. Precipitate Morphologies as an Indication of Chemistry

The mineral formation conditions in the plots can be interpreted from the SEM observations. The meniscus cements forming at grain contacts in Figure 3A,B suggest low water content at the time of precipitation; mineral nucleation occurred in boundary layer water at point contacts followed by voids being in-filled with cement (Figure 3C,D). The layer of material aligned with the underlying chrysotile fibers in Figure 4A is likely a product of incongruent dissolution during chemical weathering. A difference in activation energy between magnesium and silicon in the serpentine crystal structure means that the Mg-rich, octahedrally coordinated brucite layers are dissolved more readily than the tetrahedral siloxane (Si-rich) layers [60–65]. Non-stoichiometric leaching causes magnesium to be removed from the crystal structure at a rate up to an order of magnitude faster than silica [63]. Mg-depletion generates a porous framework of the residual siloxane layers, which collapses to produce nano-fibriform silica through a solid-state transformation instead of dissolution and re-precipitation [62]. As silica does not readily remain in solution, any dissolved silica produced during chemical weathering of the chrysotile fibers likely re-precipitated to form textures such as the botryoidal phase in Figure 4B or the amorphous desiccation crust found in the 2 cm pyroaurite horizon in the Chem-plot (Figure 4C,D). The anhedral, platy morphology exhibited by pyroaurite in Figure 5A,B is similar to that observed by Taylor et al. [66], and the presence of this phase suggests the

prevalence of a carbon-limited environment (discussed below) [48]; however, sufficient carbon was present to precipitate the observed hydromagnesite (Figure 5C,D).

#### 4.2. Mineral Carbonation Success

The hydromagnesite abundance increased in the 2–4 cm sample of the Bio-plot to contain 1.9 wt % hydromagnesite (Table 1). The low abundances of hydromagnesite, pyroaurite, and brucite compared to serpentine make it difficult to compare the behaviour of these phases between the experimental plots because the uncertainty on refined wt % abundances increases with decreasing mineral abundance using this technique [21]. This challenge could be overcome in future studies by using magnesium and carbon isotopes to, respectively, track the conversion of silicate minerals and atmospheric CO<sub>2</sub> to carbonate mineral phases. Normalizing the mole fraction of Mg in each of these minerals to that contained in serpentine reveals general trends (Figure 7). When compared to both the unreacted tailings (Figure 7C) and the Chem-plot (Figure 7B), the 2–4 cm sample from the Bio-plot (Figure 7A) shows enrichment in Mg-content in hydromagnesite with a comparable amount of Mg being found in hydromagnesite and pyroaurite. In spite of this, the inability of either plot to reach its full carbonation potential suggests the presence of a limiting condition.

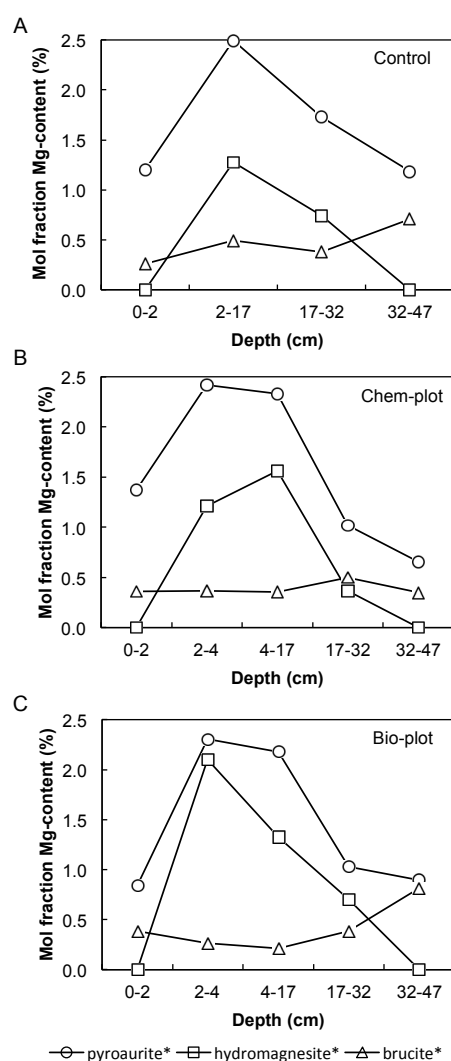


**Figure 7.** Mole fraction of the Mg content in pyroaurite, hydromagnesite, and brucite in the (A) unreacted, control tailings; (B) Chem-plot; and (C) Bio-plot.

#### 4.3. Water as a Limiting Factor

Water is required for microbial carbonation of mine tailings; it acts as a solvent for carrying ions, as a reactant to be incorporated into the crystal structure of hydrated Mg-carbonate minerals, and it is necessary for microbial survival. Schaefer et al. [67], Assima et al. [68], and Harrison et al. [69] demonstrated that limited water availability can inhibit hydrated Mg-carbonate mineral precipitation from brucite. Furthermore, Assima, Larachi, Beaudoin and Molson [68] and Harrison, Dipple, Power and Mayer [69] have shown that there is an optimal range of pore-water saturation for carbonation of brucite. The water (40 L) added to each plot plus the rainfall (248 mm) should have been sufficient for complete carbonation, assuming 100% reaction of the acid treatment. However, the observed surface runoff suggests incomplete infiltration of the full 0.5 m<sup>3</sup> volume of each plot, likely caused by the fibrous morphology of the tailings. Although the total solution volume was sufficient for carbonation, it is unlikely that the water was available for carbonate precipitation reactions at depth. Limited infiltration would confine magnesium ions to the top of the tailings, causing its transport to the surface via evaporation-induced capillary rise. Over 37 mm of rain fell 5 days after the Bio-plot was inoculated, potentially washing microbes and dissolved magnesium out of the plot. Water infiltration could be better understood by monitoring the moisture levels within the tailings pile. Dehydration and heat were likely stressors for the microorganisms during the subsequent 16-day period of no precipitation and air temperatures reaching 39 °C. The endolithic habitat provided some protection; cyanobacteria were successfully cultured from the 11-week Bio-plot 0–2 cm and 2–4 cm tailing samples (Figure 6) with no cyanobacteria recovered from the Chem-plot.

#### 4.4. Carbon as a Limiting Factor

A benefit of cyanobacterial mineral carbonation is photosynthetically generated alkalinity that increases the pH and induces carbonate mineral supersaturation. Alkalinity generation as dissolved inorganic carbon by cyanobacteria-heterotroph associations provides an indirect pathway for transferring atmospheric CO<sub>2</sub> to the tailing pore waters [36,39,40,70,71]. Limited microbial growth in the Bio-plot means that photosynthesis, and therefore alkalinity production, was underutilized under the harsh environmental conditions. This is critical for low permeability tailings because infiltration of atmospheric CO<sub>2</sub> is a known limiting factor [9]. Additionally, exopolymer production is diurnally linked to photosynthesis and active growth; restricted photosynthesis reduces the potential for the biofilm to provide carbonate mineral nucleation sites [42]. The formation of the pyroaurite horizon suggests the slow ingress of atmospheric CO<sub>2</sub> into tailings pore water [48]. The increased tendency of aqueous Mg to form hydromagnesite rather than pyroaurite and brucite in the Bio-plot (Figure 7), combined with an apparent suppression of the brucite content in the Bio-plot from 2–4 cm and 4–17 cm, suggests the Bio-plot suffered less carbon limitation than the Chem-plot. The availability of carbon could be better understood by in situ monitoring of CO<sub>2</sub> in the tailings during future tailing carbonation experiments. The challenge of carbon limitation could be amended in such experiments by increasing active microbial growth.

#### 4.5. Carbonation: Maximizing Tailings Stabilization versus Carbon Sequestration

Subsurface endolithic cyanobacteria have been previously found in carbonate crusts from Woodsreef Mine [28]. The increased abundance of hydromagnesite in the 2–4 cm Bio-plot samples combined with the recovery of cyanobacteria suggests that a protective endolithic habitat was developing. Nonetheless, a well consolidated crust such as that produced in the laboratory in 4 weeks by McCutcheon, Wilson and Southam [28] was not observed. Endolithic biofilm establishment would have enabled the production of exopolymer capable of retaining water during dry spells, and cations (Mg<sup>2+</sup>) during rain events, while also providing carbonate mineral nucleation sites [39,41–43,72–75].

Refining the deployment strategy would better utilize the microbial influence on mineral carbonation, potentially generating a carbonate crust capable of stabilizing the hazardous tailings,

reducing off-site transport of the tailings, and contamination of nearby waterways with asbestos fibers [22]. Additionally, magnesium carbonate minerals generated from acid-leached ultramafic minerals can trap and store transition metals, reducing the possibility of these metals being transported off site [76]. The potential health benefits of carbonating chrysotile fibers have been previously noted by Pronost, Beaudoin, Lemieux, Hébert, Constantin, Marcouiller, Klein, Duchesne, Molson, Larchi and Maldague [15]. Additionally, preliminary soil development through the establishment of an endolithic community of microbes and introduction of C, N, and P to the surface of the tailings would aid site remediation [28,77,78]. Nutrient availability is a limiting factor for successful revegetation of chrysotile tailings [79,80] making the early stages of soil formation vital to mine-site rehabilitation. Irrigating the acid-treated tailings could resolve the water limitations observed and allow for better growth of the microbial inoculum.

The design of this experiment was based on a successful laboratory study [28] in which acid weathering and microbial carbonation of chrysotile produced a carbonate crust. The present study demonstrated the challenges of 'on-site' implementation of mineral carbonation. Severe wetting and drying, and high temperatures were deleterious to microbial growth. Although evaporation can be a driving force for carbonate formation in arid environments [81], lack of water can be a limiting factor for hydrated carbonate mineral precipitation [69], particularly when carbonation is dependent on abundant, active cyanobacterial growth. In arid environments, and for mine sites hosting non-hazardous ultramafic tailings, it may be advantageous to target maximum carbon sequestration rather than tailings stabilization through carbonate crust formation. Constructing carbonate precipitation bioreactors such as those proposed by Power, Wilson, Small, Dipple, Wan and Southam [5] and modelled in the laboratory by McCutcheon, Power, Harrison, Dipple and Southam [43] could achieve greater carbon sequestration. Large-scale leaching of the tailings could deliver Mg-rich solutions to wetlands containing alkalinity-generating microbial mats [19]. Mine pits at derelict mines could be reengineered for this purpose, and these mineral carbonation technologies could be integrated with those targeting biofuel production [82,83]. Selecting an acid treatment that will be sufficiently neutralized during chemical weathering of the tailing minerals necessitates mineralogical characterization of the tailings [65]. Secondary carbonate minerals generated through passive carbonation of older tailings make recently milled tailings a preferred leaching target. Accounting for secondary carbonate phases or carbonate gangue minerals, such as the trace amounts of calcite in the Woodsreef tailings (Table 1), would enable more effective acid treatment of ultramafic tailings prior to mineral carbonation. Using atmospheric CO<sub>2</sub> and cyanobacteria-generated alkalinity in a carbon sequestration process is advantageous in remote locations lacking economically practical sources of CO<sub>2</sub> such as flue gases from power generation. At mine sites located in close proximity to point sources of CO<sub>2</sub>, injection of supercritical or gaseous CO<sub>2</sub> into the tailings may provide a more effective sequestration strategy [20,29,69]. Regardless of the mechanism utilized, further in situ experiments are necessary in order to optimize mineral carbonation, and must consider the environmental and mine-site parameters and challenges highlighted by the results of the present study.

## 5. Conclusions

This investigation provides the first application of microbially mediated carbonate mineral precipitation to the stabilization of asbestos mine tailings. An endolithic, phototrophic microbial community aided the increase of hydromagnesite abundance within the top few centimeters of the tailings. Unfavorable weather conditions caused water and carbon limitations in the tailings, which in turn restricted carbonate mineral precipitation. The difficulty of deploying mineral carbonation at a mine site becomes apparent when the results of this 11-week experiment are compared to those of a 4-week laboratory experiment that generated a well consolidated carbonate crust [28]. The results of the present study revealed useful information about mine-site microbial carbonation that can be used to develop a more effective strategy for deploying this method of carbonate formation for the purpose

of containing hazardous asbestos tailings. Alternatively, construction of wetland bioreactors could maximize carbon sequestration via mineral carbonation of ultramafic waste.

**Supplementary Materials:** The following are available online at [www.mdpi.com/2075-163X/7/10/191/s1](http://www.mdpi.com/2075-163X/7/10/191/s1), Figure S1: Maximum air temperature (°C) and precipitation (mm) over the duration of the experiment as measured in a nearby town, Table S1: Cation (ppm) and nutrient concentrations (ppb) in the creek water added to the experimental plots, Table S2: Rietveld results and corresponding  $R_{wp}$  values for the control tailings.  $R_{wp}$  is the weighted pattern index, a function of the least-squares residual, Table S3: Rietveld results and corresponding  $R_{wp}$  values for the tailings sampled after 2 weeks following acid leaching.  $R_{wp}$  is the weighted pattern index, a function of the least-squares residual, Table S4: Rietveld results and corresponding  $R_{wp}$  values for the tailings sampled after 11 weeks following leaching.  $R_{wp}$  is the weighted pattern index, a function of the least-squares residual.

**Acknowledgments:** We acknowledge financial support from Carbon Management Canada and the New South Wales Department of Industry to S.W. and G.S. Student support was provided to J.M. by a Natural Science and Engineering Research Council of Canada (NSERC) Post Graduate Scholarship. We thank K. Maddison, N. Staheyeff, C. Karpel, and B. Mullard of NSW Department of Industry for their support of our work at Woodsreef, with particular thanks to K.M., Project Manager for Woodsreef, for her knowledgeable advice. For their assistance in the field, we thank J. Shuster, J. Sadler, and M. Siegrist. Electron microscopy was completed at the UQ Centre for Microscopy and Microanalysis. X-ray diffraction patterns were collected at the Monash X-ray Platform.

**Author Contributions:** J.M., S.W., and G.S. conceived and designed the experiments; J.M. and G.S. performed the experiments; all authors processed the samples; all authors analyzed the data; J.M. wrote the paper with intellectual contributions made by all other authors.

**Conflicts of Interest:** The authors declare no conflict of interest. The funding sponsors had no role in the design of the study; in the collection, analyses, or interpretation of data; in the writing of the manuscript, and in the decision to publish the results.

## References

1. Lackner, K.S. A guide to CO<sub>2</sub> sequestration. *Science* **2003**, *300*, 1677–1678. [[CrossRef](#)] [[PubMed](#)]
2. Lackner, K.S.; Wendt, C.H.; Butt, D.P.; Joyce, E.L.; Sharp, D.H. Carbon-dioxide disposal in carbonate minerals. *Energy* **1995**, *20*, 1153–1170. [[CrossRef](#)]
3. Seifritz, W. CO<sub>2</sub> disposal by means of silicates. *Nature* **1990**, *345*, 486. [[CrossRef](#)]
4. Power, I.M.; Dipple, G.M.; Southam, G. Bioleaching of ultramafic tailings by *Acidithiobacillus* spp. For CO<sub>2</sub> sequestration. *Environ. Sci. Technol.* **2010**, *44*, 456–462. [[CrossRef](#)] [[PubMed](#)]
5. Power, I.M.; Wilson, S.A.; Small, D.P.; Dipple, G.M.; Wan, W.; Southam, G. Microbially mediated mineral carbonation: Roles of phototrophy and heterotrophy. *Environ. Sci. Technol.* **2011**, *45*, 9061–9068. [[CrossRef](#)] [[PubMed](#)]
6. Thom, J.G.M.; Dipple, G.M.; Power, I.M.; Harrison, A.L. Chrysotile dissolution rates: Implications for carbon sequestration. *Appl. Geochem.* **2013**, *35*, 244–254. [[CrossRef](#)]
7. Wilson, S.A.; Dipple, G.M.; Power, I.M.; Barker, S.L.L.; Fallon, S.J.; Southam, G. Subarctic weathering of mineral wastes provides a sink for atmospheric CO<sub>2</sub>. *Environ. Sci. Technol.* **2011**, *45*, 7727–7736. [[CrossRef](#)] [[PubMed](#)]
8. Wilson, S.A.; Dipple, G.M.; Power, I.M.; Thom, J.M.; Anderson, R.G.; Raudsepp, M.; Gabite, J.E.; Southam, G. Carbon dioxide fixation within mine wastes of ultramafic-hosted ore deposits: Examples from the Clinton Creek and Cassiar chrysotile deposits, Canada. *Econ. Geol.* **2009**, *104*, 95–112. [[CrossRef](#)]
9. Wilson, S.A.; Harrison, A.L.; Dipple, G.M.; Power, I.M.; Barker, S.L.L.; Mayer, U.K.; Fallon, S.J.; Raudsepp, M.; Southam, G. Offsetting of CO<sub>2</sub> emissions by air capture in mine tailings at the Mount Keith Nickel Mine, Western Australia: Rates, controls and prospects for carbon neutral mining. *Int. J. Greenhouse Gas Control* **2014**, *25*, 121–140. [[CrossRef](#)]
10. Kelemen, P.B.; Matter, J. In situ carbonation of peridotite for CO<sub>2</sub> storage. *Proc. Natl. Acad. Sci. USA* **2008**, *104*, 17295–17300. [[CrossRef](#)]
11. Kelemen, P.B.; Matter, J.; Streit, E.E.; Rudge, J.F.; Curry, W.B.; Blusztajn, J. Rates and mechanisms of mineral carbonation in peridotite- natural processes and recipes for enhanced, in situ CO<sub>2</sub> capture and storage. *Annu. Rev. Earth Planet. Sci.* **2011**, *39*, 545–576. [[CrossRef](#)]

12. Paukert, A.N.; Matter, J.M.; Kelemen, P.B.; Shock, E.L.; Havig, J.R. Reaction path modeling of enhanced in situ CO<sub>2</sub> mineralization for carbon sequestration in the peridotite of the Samail Ophiolite, Sultanate of Oman. *Chem. Geol.* **2012**, *330–331*, 86–100. [[CrossRef](#)]
13. Pronost, J.; Beaudoin, G.; Tremblay, J.; Larachi, F.; Duchesne, J.; Hébert, R.; Constantin, M. Carbon sequestration kinetic and storage capacity of ultramafic mining waste. *Environ. Sci. Technol.* **2011**, *45*, 9413–9420. [[CrossRef](#)] [[PubMed](#)]
14. Harrison, A.L.; Power, I.M.; Dipple, G.M. Accelerated carbonation of brucite in mine tailings for carbon sequestration. *Environ. Sci. Technol.* **2013**, *47*, 126–134. [[CrossRef](#)] [[PubMed](#)]
15. Pronost, J.; Beaudoin, G.; Lemieux, J.-M.; Hébert, R.; Constantin, M.; Marcouiller, S.; Klein, M.; Duchesne, J.; Molson, J.W.; Larchi, F.; et al. CO<sub>2</sub>-depleted warm air venting from chrysotile milling waste (Thetford Mines, Canada): Evidence for in-situ carbon capture from the atmosphere. *Geology* **2012**, *40*, 275–278. [[CrossRef](#)]
16. Bea, S.A.; Wilson, S.A.; Mayer, K.U.; Dipple, G.M.; Power, I.M.; Gamazo, P. Reactive transport modeling of natural carbon sequestration in ultramafic mine tailings. *Vadose Zone J.* **2012**, *11*. [[CrossRef](#)]
17. Oskierski, H.C.; Dlugogorski, B.Z.; Jacobsen, G. Sequestration of atmospheric CO<sub>2</sub> in chrysotile mine tailings of the Woodsreef Asbestos Mine, Australia: Quantitative mineralogy, isotopic fingerprinting and carbonation rates. *Chem. Geol.* **2013**, *358*, 156–169. [[CrossRef](#)]
18. Lechat, K.; Lemieux, J.-M.; Molson, J.; Beaudoin, G.; Hébert, R. Field evidence of CO<sub>2</sub> sequestration by mineral carbonation in ultramafic milling wastes, Thetford Mines, Canada. *Int. J. Greenh. Gas Control* **2016**, *47*, 110–121. [[CrossRef](#)]
19. Power, I.; McCutcheon, J.; Harrison, A.; Wilson, S.; Dipple, G.; Kelly, S.; Southam, C.; Southam, G. Strategizing carbon-neutral mines: A case for pilot projects. *Minerals* **2014**, *4*, 399–436. [[CrossRef](#)]
20. Assima, G.P.; Larachi, F.; Beaudoin, G.; Molson, J. Dynamics of carbon dioxide uptake in chrysotile mining residues—Effect of mineralogy and liquid saturation. *Int. J. Greenh. Gas Control* **2013**, *12*, 124–135. [[CrossRef](#)]
21. Wilson, S.A.; Raudsepp, M.; Dipple, G.M. Verifying and quantifying carbon fixation in minerals from serpentine-rich mine tailings using the Rietveld method with X-ray powder diffraction data. *Am. Mineral.* **2006**, *91*, 1331–1341. [[CrossRef](#)]
22. Koumantakis, E.; Kalliopi, A.; Dimitrios, K.; Gidaracos, E. Asbestos pollution in an inactive mine: Determination of asbestos fibers in the deposit tailings and water. *J. Hazard. Mater.* **2009**, *167*, 1080–1088. [[CrossRef](#)] [[PubMed](#)]
23. Assima, G.P.; Larachi, F.; Molson, J.; Beaudoin, G. Comparative study of five Quebec ultramafic mining residues for use in direct ambient carbon dioxide mineral sequestration. *Chem. Eng. J.* **2014**, *245*, 56–64. [[CrossRef](#)]
24. Turci, F.; Favero-Longo, S.E.; Gazzano, C.; Tomatis, M.; Gentile-Garofalo, L.; Bergamini, M. Assessment of asbestos exposure during a simulated agricultural activity in the proximity of the former asbestos mine of Balangero, Italy. *J. Hazard. Mater.* **2016**, *308*, 321–327. [[CrossRef](#)] [[PubMed](#)]
25. Levitan, D.M.; Hammarstrom, J.M.; Gunter, M.E.; Li, S.; Robert, R.; Chou, I.; Piatak, N.M. Mineralogy of mine waste at the Vermont asbestos group mine, Belvidere Mountain, Vermont. *Am. Mineral.* **2009**, *94*, 1063–1066. [[CrossRef](#)]
26. Vignaroli, G.; Ballirano, P.; Belardi, G.; Rossetti, F. Asbestos fibre identification vs. Evaluation of asbestos hazard in ophiolitic rock mélanges, a case study from the Ligurian Alps (Italy). *Environ. Earth Sci.* **2014**, *72*, 3679–3698. [[CrossRef](#)]
27. Vignaroli, G.; Rossetti, F.; Belardi, G.; Billi, A. Linking rock fabric to fibrous mineralisation: A basic tool for the asbestos hazard. *Nat. Hazards Earth Syst. Sci.* **2011**, *11*, 1267–1280. [[CrossRef](#)]
28. McCutcheon, J.; Wilson, S.A.; Southam, G. Microbially accelerated carbonate mineral precipitation as a strategy for in situ carbon sequestration and rehabilitation of asbestos mine sites. *Environ. Sci. Technol.* **2016**, *50*, 1419–1427. [[CrossRef](#)] [[PubMed](#)]
29. Pasquier, L.-C.; Mercier, G.; Blais, J.-F.; Cecchi, E.; Kentish, S. Parameters optimization for direct flue gas CO<sub>2</sub> capture and sequestration by aqueous mineral carbonation using activated serpentinite based mining residue. *Appl. Geochem.* **2014**, *50*, 66–73. [[CrossRef](#)]
30. Kemache, N.; Pasquier, L.-C.; Mouedhen, I.; Cecchi, E.; Blais, J.-F.; Mercier, G. Aqueous mineral carbonation of serpentinite on a pilot scale: The effect of liquid recirculation on CO<sub>2</sub> sequestration and carbonate precipitation. *Appl. Geochem.* **2016**, *67*, 21–29. [[CrossRef](#)]

31. Drew, G.H. On the precipitation of calcium carbonate in the sea by marine bacteria, and on the action of denitrifying bacteria in tropical and temperate seas. *J. Mar. Biol. Assoc. U. K.* **1913**, *9*, 479–524. [[CrossRef](#)]
32. Power, I.M.; Wilson, S.A.; Thom, J.M.; Dipple, G.M.; Southam, G. Biologically induced mineralization of dypingite by cyanobacteria from an alkaline wetland near Atlin, British Columbia, Canada. *Geochem. Trans.* **2007**, *8*, 13. [[CrossRef](#)] [[PubMed](#)]
33. Thompson, J.B.; Ferris, F.G. Cyanobacterial precipitation of gypsum, calcite, and magnesite from natural alkaline water. *Geology* **1990**, *18*, 995–998. [[CrossRef](#)]
34. Riding, R. Microbial carbonates: The geological record of calcified bacterial-algal mats and biofilms. *Sedimentology* **2000**, *47*, 179–214. [[CrossRef](#)]
35. Riding, R. Cyanobacterial calcification, carbon dioxide concentrating mechanisms, and Proterozoic-Cambrian changes in atmospheric composition. *Geobiology* **2006**, *4*, 299–316. [[CrossRef](#)]
36. Aloisi, G. The calcium carbonate saturation state in cyanobacterial mats throughout Earth's history. *Geochim. Cosmochim. Acta* **2008**, *72*, 6037–6060. [[CrossRef](#)]
37. Ferris, F.G.; Phoenix, V.; Fujita, Y.; Smith, R.W. Kinetics of calcite precipitation induced by ureolytic bacteria at 10 to 20 °C in artificial groundwater. *Geochim. Cosmochim. Acta* **2004**, *68*, 1701–1710. [[CrossRef](#)]
38. Mitchell, A.C.; Ferris, F.G. The influence of *Bacillus pasteurii* on the nucleation and growth of calcium carbonate. *Geomicrobiol. J.* **2006**, *23*, 213–226. [[CrossRef](#)]
39. Dupraz, C.; Reid, R.P.; Braissant, O.; Decho, A.W.; Norman, R.S.; Visscher, P.T. Processes of carbonate precipitation in modern microbial mats. *Earth-Sci. Rev.* **2009**, *96*, 141–162. [[CrossRef](#)]
40. Visscher, P.T.; Stolz, J.F. Microbial mats as bioreactors: Populations, processes, and products. *Palaeogeogr. Palaeoclimatol. Palaeoecol.* **2005**, *219*, 87–100. [[CrossRef](#)]
41. Braissant, O.; Decho, A.W.; Przekop, K.M.; Gallagher, K.L.; Glunk, C.; Dupraz, C.; Visscher, P.T. Characteristics and turnover of exopolymeric substances in a hypersaline microbial mat. *FEMS Microbiol. Ecol.* **2009**, *67*, 293–307. [[CrossRef](#)] [[PubMed](#)]
42. Decho, A.W.; Visscher, P.T.; Reid, R.P. Production and cycling of natural microbial exopolymers (eps) within a marine stromatolite. *Palaeogeogr. Palaeoclimatol. Palaeoecol.* **2005**, *219*, 71–86. [[CrossRef](#)]
43. McCutcheon, J.; Power, I.M.; Harrison, A.L.; Dipple, G.M.; Southam, G. A greenhouse-scale photosynthetic microbial bioreactor for carbon sequestration in magnesium carbonate minerals. *Environ. Sci. Technol.* **2014**, *48*, 9142–9151. [[CrossRef](#)] [[PubMed](#)]
44. Glen, R.A.; Butt, B.C. Chrysotile asbestos at Woodsreef, New South Wales. *Econ. Geol.* **1981**, *76*, 1153–1169. [[CrossRef](#)]
45. Cawood, P.A.; Pisarevsky, S.A.; Leitch, E.C. Unraveling the New England orocline, east Gondwana accretionary margin. *Tectonics* **2011**, *30*. [[CrossRef](#)]
46. NSW Government Trade & Investment. Woodsreef Mine Major Rehabilitation Project. Available online: <http://www.resourcesandenergy.nsw.gov.au/miners-and-explorers/programs-and-initiatives/derelect/woodsreef-mine-major-rehabilitation-project> (accessed on 30 July 2014).
47. Brown, R.E.; Brownlow, J.W.; Krynen, J.P. *Manilla–Narrabri 1:250 000 Metallogenic Map sh/56–9, sh/55–12: Metallogenic Study and Mineral Deposit Data Sheets*; Geological Survey of New South Wales, Department of Mineral Resources: Sydney, Australia, 1992.
48. Turvey, C.C.; Wilson, S.A.; Hamilton, J.L.; Southam, G. Field-based accounting of CO<sub>2</sub> sequestration in ultramafic mine wastes using portable X-ray diffraction. *Am. Mineral.* **2017**, *102*, 1302–1310. [[CrossRef](#)]
49. Vonshak, A. Laboratory techniques for the cultivation of microalgae. In *CRC Handbook of Microalgae Mass Culture*; Richmond, A., Ed.; CRC Press Inc.: Boca Raton, FL, USA, 1986; p. 117.
50. Bureau of Meteorology. Barraba, New South Wales 2016 Daily Weather Observations. Available online: <http://www.bom.gov.au/climate/dwo/IDCJDW2010.latest.shtml> (accessed on 10 February 2016).
51. Lahav, O.; Morgan, B.E.; Loewenthal, R.E. Measurement of pH, alkalinity and acidity in ultra-soft waters. *Water SA* **2001**, *27*, 423–431. [[CrossRef](#)]
52. Bruker AXS. *Topas v. 3.0: General Profile and Structure Analysis Software for Powder Diffraction Data*; Bruker AXS: Karlsruhe, Germany, 2004.
53. Rietveld, H.M. A profile refinement method for nuclear and magnetic structures. *J. Appl. Crystallogr.* **1969**, *2*, 65–71. [[CrossRef](#)]
54. Bish, D.L.; Howard, S.A. Quantitative phase analysis using the Rietveld method. *J. Appl. Crystallogr.* **1988**, *21*, 86–91. [[CrossRef](#)]

55. Hill, R.; Howard, C. Quantitative phase analysis from neutron powder diffraction data using the Rietveld method. *J. Appl. Crystallogr.* **1987**, *20*, 467–474. [[CrossRef](#)]
56. Cheary, R.W.; Coelho, A. A fundamental parameters approach to X-ray line-profile fitting. *J. Appl. Crystallogr.* **1992**, *25*, 109–121. [[CrossRef](#)]
57. Pawley, G. Unit-cell refinement from powder diffraction scans. *J. Appl. Crystallogr.* **1981**, *14*, 357–361. [[CrossRef](#)]
58. Falini, G.; Foresti, E.; Gazzano, M.; Gualtieri, A.F.; Leoni, M.; Lesci, I.G.; Roveri, N. Tubular-shaped stoichiometric chrysotile nanocrystals. *Chemistry* **2004**, *10*, 3043–3049. [[CrossRef](#)] [[PubMed](#)]
59. Wilson, S.A.; Raudsepp, M.; Dipple, G.M. Quantifying carbon fixation in trace minerals from processed kimberlite: A comparative study of quantitative methods using X-ray powder diffraction data with applications to the Diavik Diamond Mine, Northwest Territories, Canada. *Appl. Geochem.* **2009**, *24*, 2312–2331. [[CrossRef](#)]
60. Gronow, J.R. The dissolution of asbestos fibres in water. *Clay Miner.* **1987**, *22*, 21–35. [[CrossRef](#)]
61. Morgan, A. Acid leaching studies of chrysotile asbestos from mines in the Coalinga region of California and from Quebec and British Columbia. *Ann. Occup. Hyg.* **1997**, *41*, 249–268. [[CrossRef](#)]
62. Wang, L.; Lu, A.; Wang, C.; Zheng, X.; Zhao, D.; Liu, R. Nano-fibriform production of silica from natural chrysotile. *J. Colloid Interface Sci.* **2006**, *295*, 436–439. [[CrossRef](#)] [[PubMed](#)]
63. Rozalen, M.; Huertas, F.J. Comparative effect of chrysotile leaching in nitric, sulfuric and oxalic acids at room temperature. *Chem. Geol.* **2013**, *352*, 134–142. [[CrossRef](#)]
64. Park, A.-H.A.; Fan, L.-S. CO<sub>2</sub> mineral sequestration: Physically activated dissolution of serpentine and pH swing process. *Chem. Eng. Sci.* **2004**, *59*, 5241–5247. [[CrossRef](#)]
65. McCutcheon, J.; Dipple, G.M.; Wilson, S.A.; Southam, G. Production of magnesium-rich solutions by acid leaching of chrysotile: A precursor to field-scale deployment of microbially enabled carbonate mineral precipitation. *Chem. Geol.* **2015**, *413*, 119–131. [[CrossRef](#)]
66. Taylor, H.M.; Hansen, H.C.B.; Stanger, G.; Bender Koch, C. On the genesis and composition of natural pyroaurite. *Clay Miner.* **1991**, *26*, 297–309. [[CrossRef](#)]
67. Schaef, H.T.; Windisch, C.F., Jr.; McGrail, B.P.; Martin, P.F.; Rosso, K.M. Brucite [Mg(OH)<sub>2</sub>] carbonation in wet supercritical CO<sub>2</sub>: An in situ high pressure X-ray diffraction study. *Geochim. Cosmochim. Acta* **2011**, *75*, 7458–7471. [[CrossRef](#)]
68. Assima, G.P.; Larachi, F.; Beaudoin, G.; Molson, J. CO<sub>2</sub> sequestration in chrysotile mining residues—Implication of watering and passivation under environmental conditions. *Ind. Eng. Chem. Res.* **2012**, *51*, 8726–8734. [[CrossRef](#)]
69. Harrison, A.L.; Dipple, G.M.; Power, I.M.; Mayer, K.U. Influence of surface passivation and water content on mineral reactions in unsaturated porous media: Implications for brucite carbonation and CO<sub>2</sub> sequestration. *Geochim. Cosmochim. Acta* **2015**, *148*, 477–495. [[CrossRef](#)]
70. Altermann, W.; Kazmierczak, J.; Oren, A.; Wright, D.T. Cyanobacterial calcification and its rock-building potential during 3.5 billion years of Earth history. *Geobiology* **2006**, *4*, 147–166. [[CrossRef](#)]
71. Dupraz, C.; Visscher, P.T. Microbial lithification in marine stromatolites and hypersaline mats. *Trends Microbiol.* **2005**, *13*, 429–438. [[CrossRef](#)] [[PubMed](#)]
72. Beveridge, T.J. The bacterial surface: General considerations towards design and function. *Can. J. Microbiol.* **1988**, *34*, 363–372. [[CrossRef](#)] [[PubMed](#)]
73. Kluge, S.; Weston, J. Can a hydroxide ligand trigger a change in the coordination number of magnesium ions in biological systems? *Biochemistry* **2005**, *44*, 4877–4885. [[CrossRef](#)] [[PubMed](#)]
74. Trichet, J.; Défarge, C. Non-biologically supported organomineralization. *Bull. Inst. Oceanogr.* **1995**, *14*, 203–226.
75. Obst, M.; Dynes, J.J.; Lawrence, J.R.; Swerhone, G.D.W.; Benzerara, K.; Karunakaran, C.; Kaznatcheev, K.; Tyliszczak, T.; Hitchcock, A.P. Precipitation of amorphous CaCO<sub>3</sub> (aragonite-like) by cyanobacteria: A STXM study of the influence of eps on the nucleation process. *Geochim. Cosmochim. Acta* **2009**, *72*, 4180–4198. [[CrossRef](#)]
76. Hamilton, J.L.; Wilson, S.A.; Morgan, B.; Turvey, C.C.; Paterson, D.J.; MacRae, C.; McCutcheon, J.; Southam, G. Nesquehonite sequesters transition metals and CO<sub>2</sub> during accelerated carbon mineralisation. *Int. J. Greenh. Gas Control* **2016**, *55*, 73–81. [[CrossRef](#)]

77. Šourková, M.; Frouz, J.; Fettweis, U.; Bens, O.; Hüttl, R.F.; Šantrůčková, H. Soil development and properties of microbial biomass succession in reclaimed post mining sites near Sokolov (Czech Republic) and near Cottbus (Germany). *Geoderma* **2005**, *129*, 73–80. [[CrossRef](#)]
78. Frouz, J.; Keplin, B.; Pižl, V.; Tajovský, K.; Starý, J.; Lukešová, A.; Nováková, A.; Balík, V.R.; Háněl, L.; Materna, J.; et al. Soil biota and upper soil layer development in two contrasting post-mining chronosequences. *Ecol. Eng.* **2001**, *17*, 275–284. [[CrossRef](#)]
79. Meyer, D.R. Nutritional problems associated with the establishment of vegetation on tailings from an asbestos mine. *Environ. Pollut. Ser. A Ecol. Biol.* **1980**, *23*, 287–298. [[CrossRef](#)]
80. Moore, T.R.; Zimmermann, R.C. Establishment of vegetation on serpentine asbestos mine wastes, southeastern Quebec, Canada. *J. Appl. Ecol.* **1977**, *14*, 589–599. [[CrossRef](#)]
81. Oskierski, H.C.; Dlugogorski, B.Z.; Oliver, T.K.; Jacobsen, G. Chemical and isotopic signatures of waters associated with the carbonation of ultramafic mine tailings, Woodsreef Asbestos Mine, Australia. *Chem. Geol.* **2016**, *436*, 11–23. [[CrossRef](#)]
82. Mata, T.M.; Martins, A.A.; Caetano, N.S. Microalgae for biodiesel production and other applications: A review. *Renew. Sustain. Energy Rev.* **2010**, *14*, 217–232. [[CrossRef](#)]
83. Ramanan, R.; Kannan, K.; Deshkar, A.; Yadav, R.; Chakrabarti, T. Enhanced algal CO<sub>2</sub> sequestration through calcite deposition by *Chlorella* sp. and *Spirulina platensis* in a mini-raceway pond. *Bioresour. Technol.* **2010**, *101*, 2616–2622. [[CrossRef](#)] [[PubMed](#)]



© 2017 by the authors. Licensee MDPI, Basel, Switzerland. This article is an open access article distributed under the terms and conditions of the Creative Commons Attribution (CC BY) license (<http://creativecommons.org/licenses/by/4.0/>).